Three-Level Optimized Pulse Patterns With Reduced Common-Mode Voltage

Isavella Koukoula
Faculty of Inf. Technol. and Commun. Sciences
Tampere University
Tampere, Finland
isavella.koukoula@tuni.fi

Petros Karamanakos
Faculty of Inf. Technol. and Commun. Sciences
Tampere University
Tampere, Finland
p.karamanakos@ieee.org

Tobias Geyer
ABB System Drives
ABB Switzerland Ltd
Turgi, Switzerland
t.geyer@ieee.org

***Abstract*—This paper proposes the computation of three-level optimized pulse patterns (OPPs) with reduced common-mode voltage (CMV) over the whole range of modulation indices. Limiting the CMV, however, gives rise to increased current harmonics. To mitigate this, the OPP optimization problem is reformulated to allow for symmetry relaxations and multipolar switch positions. In doing so, the current harmonics not only remain low, but they are occasionally even lower than those of traditional OPPs. The presented numerical results, based on a medium-voltage (MV) drive consisting of a three-level converter and an induction machine, demonstrate the benefits of the proposed approach.**

***Index Terms*—Optimal control, Voltage Source Converter (VSC), Modulation scheme, Pulse Width Modulation (PWM), Medium voltage converter.**

I. Introduction

The three-phase output voltage of an inverter is a switched waveform with a common-mode voltage (CMV) component. CMV can increase the stress on the motor insulation and damage the bearings [1]. Hence, limiting the CMV is often a necessity.

To this aim, different modulation schemes have been proposed to minimize the CMV. Among these modulation strategies, some *completely* eliminate the CMV. For example, when considering three-level converters, different pulse width modulation (PWM) techniques have been proposed that employ only these voltage vectors that produce zero CMV [2]. However, due to the limited number of available voltage vectors, the available voltage is underutilized as the modulation index is limited to $\frac{2\sqrt{3}}{\pi}$ (out of $\frac{4}{\pi}$). In addition, as these methods use only non-adjacent voltage vectors, the harmonic distortions increase significantly. Finally, to keep the CMV at zero, at least two phases have to switch simultaneously, which may not be allowed by the hardware for protection reasons.

For the aforementioned reasons, *partial* elimination of the CMV has also been considered. In this direction, a PWM scheme with phase opposite disposition (POD-PWM) is proposed for three- and five-level converters in [3] and [4], respectively. However, the total demand distortion (TDD) of the line voltage and current is significantly increased compared with that of conventional PWM. Moreover, two phases may switch simultaneously, which may not be possible in practice, as mentioned above. As a solution to that, a modified PWM strategy with reduced CMV is proposed in [5] for a three-level converter. This technique uses four (instead of two) carriers and achieves an improved harmonic performance compared to POD-PWM. Furthermore, space vector modulation (SVM) with limited CMV has also been investigated, see e.g., [6]. Recently, a modified SVM, suitable for multilevel (including three-level) converters was proposed in [7]. This method achieves lower harmonic distortions compared to POD-PWM. Finally selective harmonic elimination (SHE) PWM can also be modified to achieve a CMV reduction. Specifically, the SHE switching angles can be computed such that they eliminate not only specific differential-mode harmonics, but also low-order triplen harmonics to reduce the CMV [8]. However, the dc-link voltage cannot be fully utilized because of the absence of low-order triplen harmonics.

Based on the above, the proposed PWM methods that keep the CMV limited suffer either from increased current distortions or underutilization of the available voltage (or both). A PWM technique that can address both issues are optimized pulse patterns (OPPs). This method, first introduced in 1977 [9], aims to reduce the harmful effects of harmonics on a machine driven by a power converter. To achieve this, the optimal PWM patterns are computed in an offline procedure that minimizes an objective function that accounts for the TDD of the stator current. Hence, OPPs can produce the theoretical minimum current TDD when applied to a machine. Moreover, OPPs can be computed for the whole range of modulation indices without requiring an explicit CMV injection. However, the OPP optimization problem does not directly address other adverse effects of the switching patterns, such as the CMV.

Motivated by the above, and as far as three-level OPPs are concerned, a few concepts have been presented that compute OPPs with limited CMV, see, e.g., [10] and [11]. The former investigates the computation of OPPs with zero CMV. To do so, a set of linear constraints is added to the traditional OPP optimization problem. Subsequently, the optimization problem is reformulated by dividing the switching angles into pairs which are appropriately constrained. However, as the dimension of the problem increases (i.e., as the number of switching angles grows), the formulation and subsequent solution of the OPP problem becomes numerically very challenging. On the other hand, [11] imposes a constraint on the sum of the triplen

harmonics. This limit, however, is heuristically chosen, thus increasing the possibility of suboptimal results.

In both of the aforementioned works, however, the limitation of the CMV occurs at the expense of increased harmonic distortions. To mitigate this issue, this paper proposes to reformulate the OPP optimization problem by dropping artificial restrictions that are adopted in the traditional OPP problem. Specifically, as recently shown in [12], by relaxing quarter-wave symmetry of the OPP and considering multipolar (instead of unipolar) switch positions, the fundamental trade-off between the current harmonic distortion and inverter switching frequency can be improved as the search space of the three-level OPP problem increases. By exploiting this, the reformulated optimization problem leads to OPPs that produce similar current TDDs as traditional OPPs, but reduce the CMV over the whole range of modulation indices. The presented numerical results for a three-level converter driving a medium-voltage (MV) induction machine verify this favorable property.

II. OPPs with Reduced Common-Mode Voltage

Assuming a three-level converter, we define the pulse number d as the ratio between the device switching frequency f_{sw} and the fundamental frequency f_1, i.e., $d = \frac{f_{\text{sw}}}{f_1}$. A 2π (i.e., full-wave) periodic switching waveform $u(\theta)$, where θ is the angle (or argument) of the pulse pattern, is fully described by $4d+1$ switch positions $u_i \in \{-1, 0, 1\}$, with $i \in \{0, \dots, 4d\}$, and $4d$ switching angles α_i, $i \in \{1, \dots, 4d\}$. At each angle α_i a switching transition $\Delta u_i = u_i - u_{i-1} \in \{-1, 1\}$ occurs. Note that due to the 2π-periodicity, the initial switch and last switch positions are the same, i.e., $u_0 = u_{4d}$.

OPPs are computed such that the output current of the inverter has as low harmonic distortions as possible. To this aim, an objective function that captures the current TDD is minimized. Assuming an inductive load, the current TDD [12] is given by

$$I_{\text{TDD}} = \frac{1}{\sqrt{2} I_{\text{nom}} \omega_1 X} \frac{V_{\text{dc}}}{2} \sqrt{\sum_{n \neq 1} \left(\frac{\hat{u}_n}{n} \right)^2} = c\sqrt{J}\,. \tag{1}$$

The constant c, which depends on the nominal current I_{nom}, angular fundamental frequency ω_1, load reactance X, and dc-link voltage V_{dc}, can be discarded as it does not affect the optimization result. Hence, the objective function J of the OPP problem accounts for the voltage harmonics $\hat{u}_n$, weighted by their harmonic order, which is proportional to the current TDD, provided that the load is inductive. Note that the amplitude of the n^{th} harmonic is given by $\hat{u}_n = \sqrt{a_n^2 + b_n^2}$, with a_n and b_n being the Fourier coefficients of the periodic OPP waveform. For the analytical expressions of the Fourier coefficients, the reader is referred to [12].

A. Traditional OPP Problem

Traditional OPPs imposes the following properties:

(P1) Three-phase symmetry, i.e., if the OPP for phase a is $u_a(\theta) = u(\theta)$, then $u_b(\theta) = u\left(\theta - \frac{2\pi}{3}\right)$ and $u_c(\theta) = u\left(\theta + \frac{2\pi}{3}\right)$ are the OPPs for phases b and c, respectively;

(P2) Half-wave symmetry, i.e., $u(\theta) = -u(\theta + \pi)\ \forall \theta \in [0, \pi]$;

(P3) Quarter-wave symmetry, i.e., $u(\theta) = u(\pi - \theta)\ \forall \theta \in \left[0, \frac{\pi}{2}\right]$;

(P4) Unipolar switching, i.e., $u(\theta) \geq 0,\ \forall \theta \in \left[0, \frac{\pi}{2}\right]$, whereas the first switch position is always zero, i.e., $u_0 = 0$.

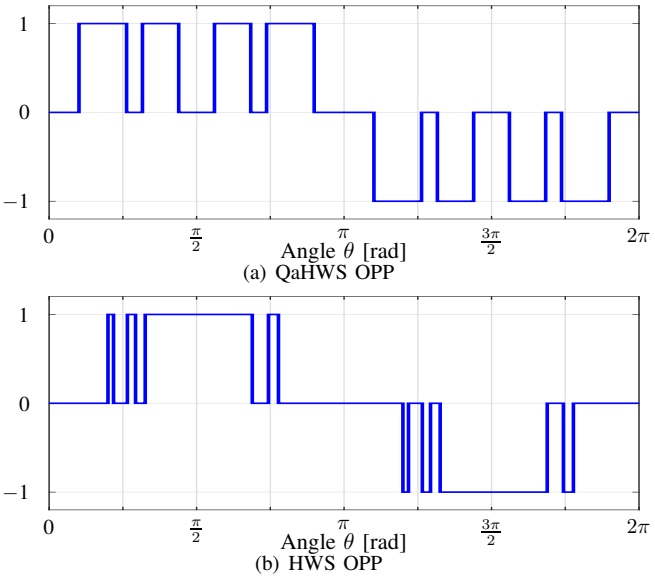

(a) QaHWS OPP

(b) HWS OPP

Fig. 1: Examples of OPPs with different symmetry properties for $d = 4$ at modulation index $m = 0.8$.

An OPP with these properties is shown in Fig. 1(a).

The above properties imply that for the computation of traditional OPPs, hereafter referred to as quarter- and half-wave symmetric (QaHWS) OPPs, only the d switching angles $\alpha_1, \dots, \alpha_d \in [0, \pi/2]$ of u_a are required to fully characterize the three-phase OPP. Hence, the corresponding optimization problem is of the form

$$\begin{aligned} \underset{\boldsymbol{\alpha}_Q}{\text{minimize}} \quad & J_1(\boldsymbol{\alpha}_Q) = \textstyle\sum_{n=5,7,\dots} \left(\frac{b_n}{n}\right)^2 \\ \text{subject to} \quad & b_1 = m \\ & 0 \leq \alpha_1 \leq \alpha_2 \leq \dots \leq \alpha_d \leq \tfrac{\pi}{2}\,, \end{aligned} \tag{2}$$

where $\boldsymbol{\alpha}_Q = [\alpha_1\ \alpha_2\ \dots\ \alpha_d]^T$, and $m \in [0, 4/\pi]$ is the desired modulation index. Note that due to the QaHWS, the a_n Fourier coefficients are zero, and only non-triplen, odd harmonics are nonzero.

B. Common Mode

The CMV is defined as the average of the three single-phase output voltages of the inverter v_x, with $x \in \{a, b, c\}$. Since it holds that $v_x = \frac{V_{\text{dc}}}{2} u_x$, it directly follows that the *common-mode (CM) switch position* u_o is defined as

$$u_o(\theta) = \frac{u_a(\theta) + u_b(\theta) + u_c(\theta)}{3}\,. \tag{3}$$

The CM switch position u_o is a $\frac{2\pi}{3}$–periodic signal, and inherits the symmetry properties of the OPP, as shown in the appendix.

Consider an OPP with HWS. This implies that the CM switch position u_o exhibits HWS as well, see the appendix. Since u_o depends on the three single-phase OPPs u_x, with $x \in \{a, b, c\}$, HWS implies that u_o can be constructed based on the information included in the three-phase OPP $\boldsymbol{u}_{abc}(\theta) = [u_a(\theta)\ u_b(\theta)\ u_c(\theta)]^T$ for $\theta \in \left[0, \frac{\pi}{3}\right]$. With the help of (P1) and (P2), the single-phase OPP in phase b can be written as

$$\begin{aligned} u_b(\theta) = u\left(\theta - \frac{2\pi}{3}\right) = u\left(\theta + \pi + \frac{\pi}{3}\right) \overset{\phi=\theta+\frac{\pi}{3}}{=} \\ u(\phi + \pi) \overset{\text{(P2)}}{=} -u(\phi) = -u\left(\theta + \frac{\pi}{3}\right),\ \theta \in \left[0, \frac{\pi}{3}\right]. \end{aligned} \tag{4}$$

It follows that u_o can be unambiguously constructed from the single-phase OPP $u(\theta)$, $\theta \in [0, \pi]$ as the following hold:

- Interval $\left[0, \frac{\pi}{3}\right] \Rightarrow u_a(\theta) = u(\theta)$, $\theta \in \left[0, \frac{\pi}{3}\right]$: The first 60°-segment of $u(\theta)$ is identical to that of $u_a(\theta)$, see the blue segment in Fig. 2.
- Interval $\left[\frac{\pi}{3}, \frac{2\pi}{3}\right] \Rightarrow u_b(\theta) = -u\left(\theta + \frac{\pi}{3}\right)$, $\theta \in \left[0, \frac{\pi}{3}\right]$: The second 60°-segment of $u(\theta)$ is identical to the first 60°-segment of $-u_b(\theta)$. This means that when a switching transition occurs in $u(\theta)$ at α_i, where $\alpha_i \in \left[\frac{\pi}{3}, \frac{2\pi}{3}\right]$, then the opposite switching transition happens in u_b at $\alpha_i - \frac{\pi}{3}$, see the red segment in Fig. 2.
- Interval $\left[\frac{2\pi}{3}, \pi\right] \Rightarrow u_c(\theta) = u\left(\theta + \frac{2\pi}{3}\right)$, $\theta \in \left[0, \frac{\pi}{3}\right]$: The third 60°-segment of $u(\theta)$ is identical to the first 60°-segment of $u_c(\theta)$. This means that when a switching transition occurs in $u(\theta)$ at α_i, where $\alpha_i \in \left[\frac{2\pi}{3}, \pi\right]$, then the same switching transition happens in u_c at $\alpha_i - \frac{2\pi}{3}$, see the green segment in Fig. 2.

In a similar fashion, if the OPP is QaHWS then u_o exhibits QaHWS too, see the appendix. Therefore, the necessary information to compute u_o is included in $\boldsymbol{u}_{abc}(\theta), \theta \in \left[0, \frac{\pi}{6}\right]$. Moreover, considering properties (P1)–(P3) and the fact that the single-phase OPP in phase c, u_c, can be written as

$$\begin{aligned} u_c(\theta) = u\left(\theta + \frac{2\pi}{3}\right) \overset{\phi=\theta+\frac{2\pi}{3}}{=} u(\phi) \overset{\text{(P3)}}{=} u(\pi - \phi) = \\ u\left(\pi - \theta - \frac{2\pi}{3}\right) = u\left(\frac{\pi}{3} - \theta\right), \end{aligned} \tag{5}$$

it can be concluded that u_o can be constructed from the single-phase OPP $u(\theta)$, $\theta \in \left[0, \frac{\pi}{2}\right]$ since the following statements apply:

- Interval $\left[0, \frac{\pi}{6}\right] \Rightarrow u_a(\theta) = u(\theta)$, $\theta \in \left[0, \frac{\pi}{6}\right]$: The first 30°-segment of $u(\theta)$ is identical to that of $u_a(\theta)$, see the blue segment in Fig. 3.
- Interval $\left[\frac{\pi}{6}, \frac{\pi}{3}\right] \Rightarrow u_c(\theta) = u\left(\frac{\pi}{3} - \theta\right)$, $\theta \in \left[0, \frac{\pi}{6}\right]$: The second 30°-segment of $u(\theta)$ is identical to the first mirrored 30°-segment of $u_c(\theta)$. This means that when a switching transition occurs in $u(\theta)$ at α_i, where $\alpha_i \in \left[\frac{\pi}{6}, \frac{\pi}{3}\right]$, then the same switching transition happens in u_c at $\frac{\pi}{3} - \alpha_i$, see the green segment in Fig. 3.

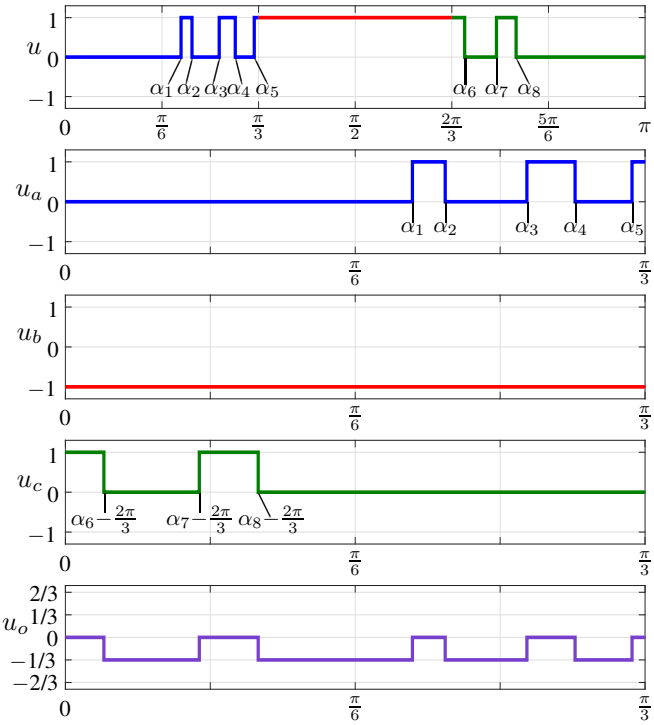

Fig. 2: Illustration of CMV calculation of HWS OPP for $d = 4$ at modulation index $m = 0.8$

- Interval $\left[\frac{\pi}{3}, \frac{\pi}{2}\right] \Rightarrow u_b(\theta) = -u\left(\theta + \frac{\pi}{3}\right)$, $\theta \in \left[0, \frac{\pi}{6}\right]$: The third 30°-segment of $u(\theta)$ is identical to the first 30°-segment of $-u_b(\theta)$. This means that when a switching transition occurs in $u(\theta)$ at α_i, where $\alpha_i \in \left[\frac{\pi}{3}, \frac{\pi}{2}\right]$, then the opposite switching transition happens in u_b at $\alpha_i - \frac{\pi}{3}$, see the red segment in Fig. 3.

C. Common-Mode Constraint

To limit the CMV to a desired level, a constraint on u_o is added to the OPP optimization problem. Assuming that property (P1) holds, the constraint is of the form

$$\begin{aligned} \max\left(|u_o(\theta)|\right) = \\ \max\left(\left|\frac{u(\theta) + u(\theta - \frac{2\pi}{3}) + u(\theta - \frac{4\pi}{3})}{3}\right|\right) \leq \frac{1}{3}, \end{aligned} \tag{6}$$

where the goal is to limit the CMV to $V_{\text{dc}}/6$. The maximum absolute value of u_o in (6) needs to be calculated during the OPP optimization process. To do so, the procedure described in Algorithm 1 is adopted. With this procedure and constraint (6), the OPP problem (2) is revised to compute QaHWS OPPs with limited CMV, as shown in Section III. Nevertheless, the introduction of (6) compromises the current TDD, as a degree of freedom in the minimization of I_{TDD} is removed, as also demonstrated in the numerical results presented in Section III. To address this issue, the optimization problem that computes OPPs with constrained CMV is reformulated, as discussed in the following section.

D. OPP Problem with Common-Mode Constraint

As recently shown in [12], relaxing the OPP properties increases the search space of the three-level OPP problem,

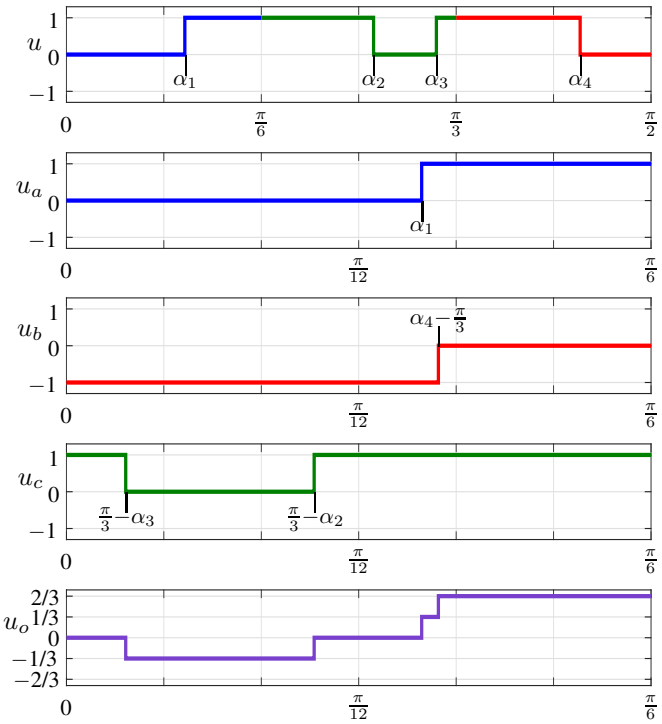

Fig. 3: Illustration of CMV calculation of QaHWS OPP for $d = 4$ at modulation index $m = 0.8$

Algorithm 1 Constraint on common-mode switch position

For OPPs with HWS:

1. Given $u(\theta)$, with $\theta \in [0, \pi]$, construct the three-phase OPP $\boldsymbol{u}_{abc}(\theta)$ for $\theta \in [0, \frac{\pi}{3}]$, as described above.
2. Sort the $2d$ switching angles of $\boldsymbol{u}_{abc}$ in ascending order.
3. Calculate u_o by cumulative summing up the corresponding switching transitions $\Delta u(\alpha_i)$ for $0 \leq \alpha_i \leq \frac{\pi}{3}$.

Return $u_o(\theta)$ for $\theta \in \left[0, \frac{\pi}{3}\right]$.

For OPPs with QaHWS:

1. Given $u(\theta)$, with $\theta \in [0, \frac{\pi}{2}]$, construct the three-phase OPP $\boldsymbol{u}_{abc}(\theta)$ for $\theta \in [0, \frac{\pi}{6}]$, as described above.
2. Sort the d switching angles of $\boldsymbol{u}_{abc}$ in ascending order.
3. Calculate u_o by cumulative summing up the corresponding switching transitions $\Delta u(\alpha_i)$ for $0 \leq \alpha_i \leq \frac{\pi}{6}$.

Return $u_o(\theta)$ for $\theta \in \left[0, \frac{\pi}{6}\right]$.

and thus the degrees of freedom during the OPP computation process. Motivated by this, in this work we relax the symmetry and switching properties, namely we drop properties (P3) and (P4). By dropping the former only HWS OPPs are considered, meaning that $2d$ switching angles need to be computed, as opposed to the d angles computed for QaHWS OPPs, see problem (2). An example of HWS OPP is depicted in Fig. 1(b).

Relaxing the unipolar switch position and $u_0 = 0$ (see property (P4)), i.e., allowing for multipolar switching, gives rise to more than one candidate pulse patterns. Specifically, as the switching transitions Δu_i assume values ± 1, only every second switch position is a degree of freedom when three-level OPPs are of interest. Therefore, when considering pulse patterns with $2d$ angles—and given that $u_{2d} = -u_0$ holds for HWS OPPs—there are:

- 2^d pulse patterns when the initial switch position is 0. From those, one pulse pattern is excluded as it includes only zero or negative switch positions in the positive half-wave of the fundamental waveform.
- 2^{d-1} pulse patterns when the initial switch position is -1 or 1, since both the first and second switch positions are fixed.

Thus, based on the above, the total number of candidate pulse patterns that need to be evaluated is $N = 2^d - 1 + 2 \cdot 2^{d-1} = 2^{d+1} - 1$, indicating an exponential increase with d. This implies that the corresponding underlying optimization problem is not only nonconvex (like (2)), but also mixed integer.

Hence, when solving the optimization problem of HWS OPPs with multipolar switching, one needs to compute not only the $2d$ optimal switching angles $\boldsymbol{\alpha}_H = [\alpha_1 \ \alpha_2 \ \ldots \ \alpha_{2d}]^T$, but also the optimal switching sequence $\boldsymbol{u}_H = [u_0 \ u_1 \ \ldots \ u_{2d-1}]^T$. Thus, the final optimization problem that accounts for the CMV constraint is

$$\begin{aligned} \underset{\boldsymbol{\alpha}_H, \boldsymbol{u}_H}{\text{minimize}} \quad & J_1(\boldsymbol{\alpha}_H, \boldsymbol{u}_H) = \textstyle\sum_{n=5,7,\ldots} \frac{a_n^2 + b_n^2}{n^2} \\ \text{subject to} \quad & a_1 = 0, \ b_1 = m \\ & 0 \leq \alpha_1 \leq \alpha_2 \leq \ldots \leq \alpha_{2d} \leq \pi \\ & u_i \in \{-1, \ 0, \ 1\} \text{ and} \\ & u_{i+1} - u_i \in \{-1, \ 1\} \ \ \forall i \in \{0, \ldots, 2d-1\} \\ & \max\left(|u_o(\theta)|\right) \leq \tfrac{1}{3} \, . \end{aligned} \tag{7}$$

Note that due to the HWS, both a_n and b_n Fourier coefficients are nonzero for the non-triplen, odd harmonics, except for the fundamental component, where it is desired that $a_1 = 0$, such that the phase of the fundamental component is zero.

III. Numerical Results

This section shows the optimization results for (a) QaHWS OPPs without limitations on the CMV (see problem (2)); (b) QaHWS with reduced CMV and (c) HWS OPPs with reduced CMV (see (7)). OPPs in the (b) category are hereafter referred to as QaHWS CMV OPPs, while those in category (c) as HWS CMV OPPs. All OPPs are computed for a MV drive system consisting of a squirrel cage induction machine with 3.3 kV rated voltage, 2.12 kA rated current, 50 Hz nominal frequency, 0.25 per unit (p.u.) total leakage reactance, and a three-level inverter with a dc-link voltage of $V_{\text{dc}} = 5.2$ kV. For demonstration purposes, OPPs with $d = 2, 3, 4, 5$ are considered.

The CMV of QaHWS OPPs with pulse numbers $d = 2$ to 5 are shown in Figs. 4(a) to 7(a), see the (blue) solid lines. As can be seen, when the CMV is not constrained, then the maximum value of the CM switch position is $\max(|u_o|) = 2/3$ for a wide range of modulation indices, namely $m \in [0.539, 1.228]$ for $d = 2$, $m \in [1.039, 1.178]$ for $d = 3$, $m \in [0.554, 1.213]$ for $d = 4$, and $m \in [0.434, 0.719] \cup [0.869, 1.193]$ for $d = 5$.

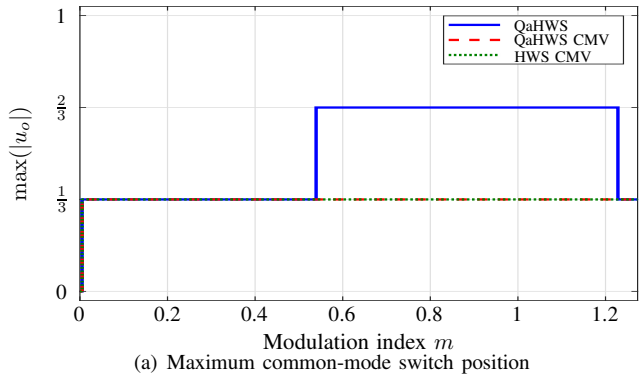

(a) Maximum common-mode switch position

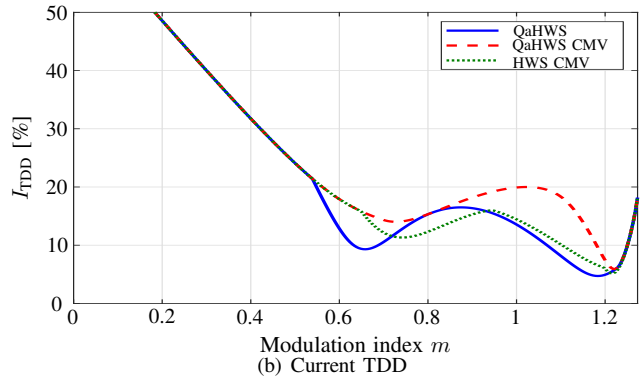

(b) Current TDD

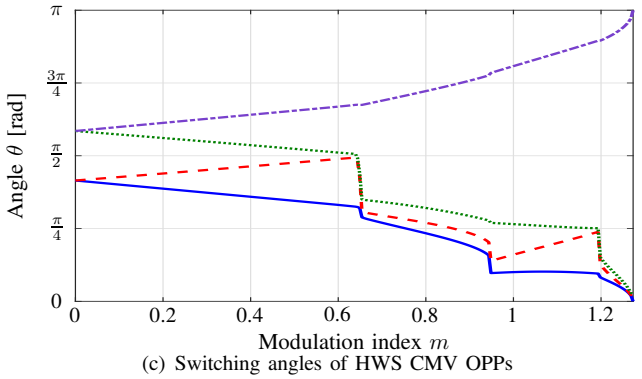

(c) Switching angles of HWS CMV OPPs

Fig. 4: QaHWS and HWS OPPs for $d = 2$ without and with the CMV constraint. The solid (blue) line corresponds to the traditional QaHWS OPPs, the dashed (green) line to QaHWS OPPs with constrained CMV (QaHWS CMV OPPs), and the dotted (red) line to HWS OPPs with constrained CMV (HWS CMV OPPs).

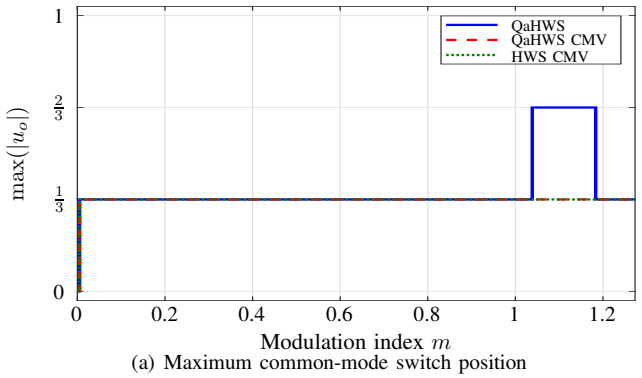

(a) Maximum common-mode switch position

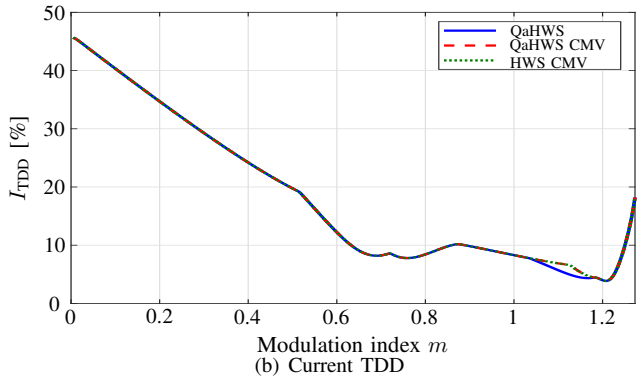

(b) Current TDD

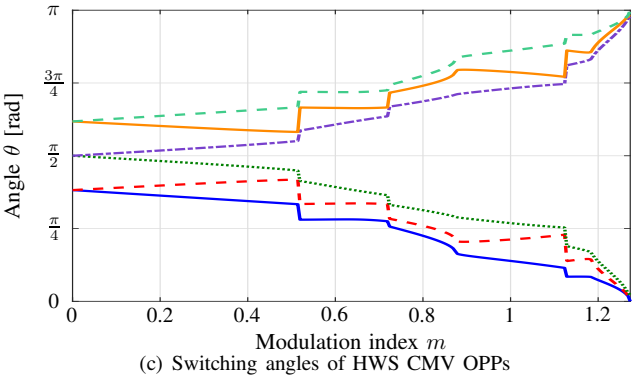

(c) Switching angles of HWS CMV OPPs

Fig. 5: QaHWS and HWS OPPs for $d = 3$ without and with the CMV constraint. The solid (blue) line corresponds to the traditional QaHWS OPPs, the dashed (green) line to QaHWS OPPs with constrained CMV (QaHWS CMV OPPs), and the dotted (red) line to HWS OPPs with constrained CMV (HWS CMV OPPs).

On the other hand, when the CMV constraint is implemented (see Section II-C), the resulting QaHWS CMV OPPs reduce the CMV for all the aforementioned values of m. This, however, occurs at a cost of an increased current TDD, as can be observed in Figs. 4(b) to 7(b). Nevertheless, it is worth noting that for even pulse numbers d, not only the CMV of HWS CMV OPPs is effectively reduced over the whole range of modulation indices, but also the current TDD is lower than that of QaHWS CMV OPPs. More importantly, when the CMV-constrained OPPs are benchmarked against traditional QaHWS OPPs, the increase in I_{TDD} caused by the limitation of CMV is relatively small in HWS CMV OPPs. Indeed, for $d = 2$ the maximum increase in I_{TDD} is only 2.33% at $m = 1.148$, whereas that caused by QaHWS CMV OPPs is 10.18% at $m = 1.104$. Similarly, for $d = 4$, the maximum increase in I_{TDD} is only 1.87% at $m = 1.044$ for HWS CMV OPPs. On the other hand, a 2.87% increase in I_{TDD} is observed at $m = 0.884$ for QaHWS CMV OPPs. More impressively, compared with traditional QaHWS OPPs, HWS CMV OPPs reduce the current TDD for $d = 2$ and modulation index range $0.724 \leq m \leq 0.929$. A similar observation can be done for HWS CMV OPPs with $d = 4$; in this case, the favorable range of modulation indices is $0.709 \leq m \leq 0.819$. This is thanks to the additional degrees of freedom of problem (7), as it can distribute $2d$ angles over a wider range of values. This point is highlighted in Figs. 4(c) and 6(c). Note that even though problem (7) can choose among several pulse patterns due to the bipolar switching to further improve the current distortions, it turns out that the resulting OPPs still have unipolar pulse patterns. Bipolar

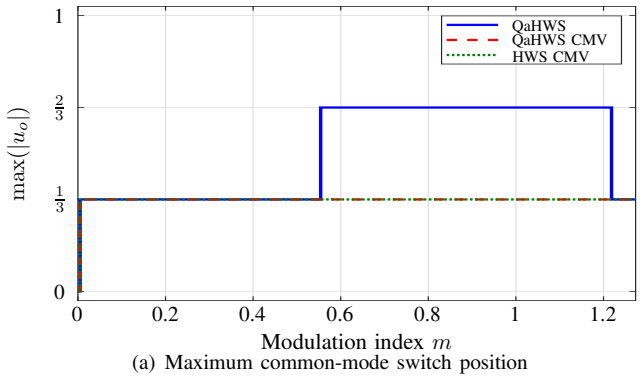

(a) Maximum common-mode switch position

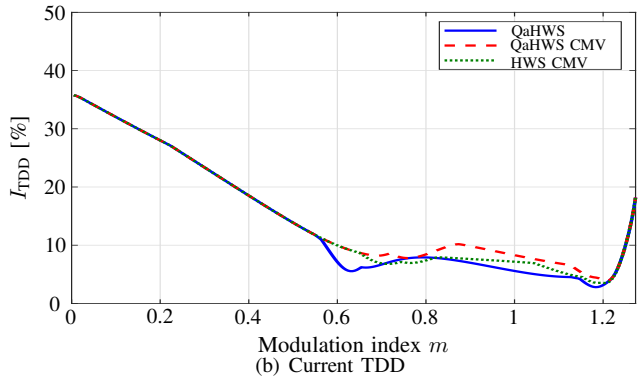

(b) Current TDD

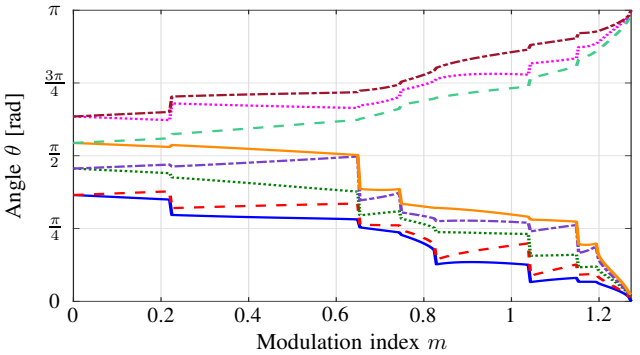

(c) Switching angles of HWS CMV OPPs

Fig. 6: QaHWS and HWS OPPs for $d = 4$ without and with the CMV constraint. The solid (blue) line corresponds to the traditional QaHWS OPPs, the dashed (green) line to QaHWS OPPs with constrained CMV (QaHWS CMV OPPs), and the dotted (red) line to HWS OPPs with constrained CMV (HWS CMV OPPs).

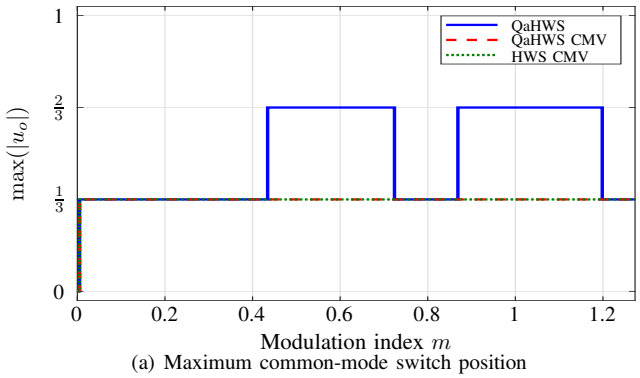

(a) Maximum common-mode switch position

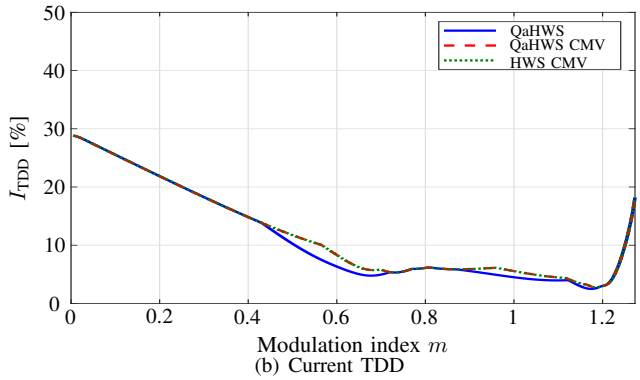

(b) Current TDD

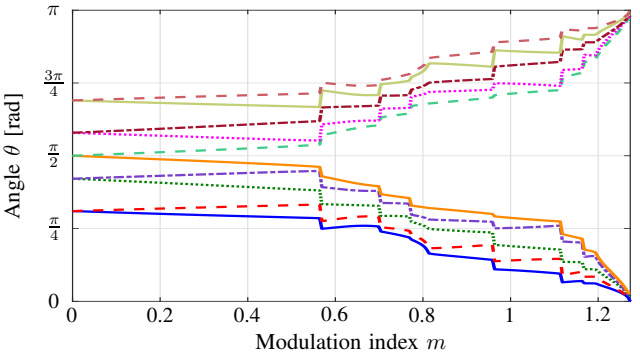

(c) Switching angles of HWS CMV OPPs

Fig. 7: QaHWS and HWS OPPs for $d = 5$ without and with the CMV constraint. The solid (blue) line corresponds to the traditional QaHWS OPPs, the dashed (green) line to QaHWS OPPs with constrained CMV (QaHWS CMV OPPs), and the dotted (red) line to HWS OPPs with constrained CMV (HWS CMV OPPs).

switching patterns have the significant advantage of choosing among all voltage vectors without the limitations imposed by unipolar switching. When imposing the CMV constraint, however, these additional degrees of freedom are foregone, as bipolar switching leads to either infeasible or suboptimal patterns.

Interestingly, below $m = 0.68$, the OPPs exhibit QaHWS, whereas above $m = 0.68$ OPPs exhibit QaHWS or HWS. Specifically, for odd pulse numbers, the relaxation of properties (P3) and (P4) does not lead to any improvements, see Figs. 5(c) and 7(c). As can be seen there, the switching angles of the HWS CMV OPPs for $d = 3$ and $d = 5$ exhibit QaHWS, with the symmetry relaxation providing no benefits.

To further elucidate this point, it is worth investigating the behavior of unipolar OPPs with and without the CMV constraint. Specifically, the pulse number determines if the switch position of QaHWS OPPs in phase a, u_a, at $\theta = \pi/2$ is 0 or 1, depending on whether d is even or odd, respectively. In the HWS OPPs, this limitation is alleviated as an unequal number of switching events between the two quarters of the half-period is allowed. The results presented in this work suggest that for odd pulse numbers d (e.g., $d = 3$ or 5), the restriction of $u_a(\frac{\pi}{2}) = 1$ respects the CMV constraint, and, therefore, lifting the quarter-wave symmetry (P3) does not lead to improved results. On the other hand, it leads to a noteworthy improvement in the current TDD in the case of $d = 2$ and 4. This implies that the relaxation of the quarter-wave symmetry (P3) is expected to lead to improved results when d is even. This is due to the limitations that QaHWS poses to the CMV-constrained OPP problem when d is even,

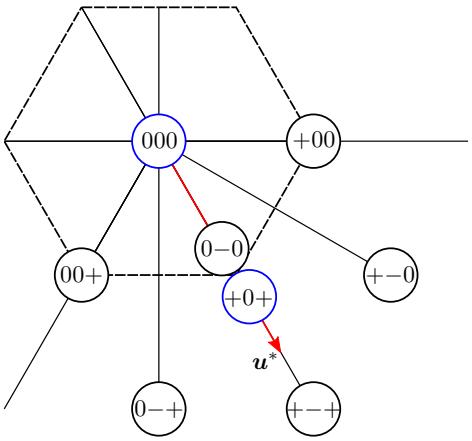

Fig. 8: Voltage vectors and corresponding three-phase switch positions of Example 1.

as explained in the following example.

Example 1. *Consider unipolar QaHWS OPP with $m > \frac{2}{3}$ at $\theta = \frac{\pi}{6}$. The fundamental component of the OPP $\boldsymbol{u}^*$ in the $\alpha\beta$-plane is shown in Fig. 8. As can be seen, $\boldsymbol{u}^*$ is aligned with the short vectors that correspond to the switch positions "0−0" and "+0+" as well as with the long vector with switch position "+−+". Based on the observations presented in the appendix, the voltage sequence for the first $\pi/6$ radians must end with a voltage vector on the symmetry axis. Additionally, note that the pulse number determines if the switch position of QaHWS OPPs in phase a, u_a, at $\theta = \pi/2$ is 0 or 1, depending on whether d is even or odd. Given the symmetry property (P2), (4) holds, this means that the phase b switch position u_b at $\theta = \pi/6$ is 0 or −1, depending on whether d is even or odd, respectively. In the former case, the possible voltage vectors that can be used to synthesize the desired modulation index require $u_b(\frac{\pi}{6}) = 0$, shown as blue circles in Fig. 8. In the unconstrained problem, the voltage vector that corresponds to "+0+" is preferred, since it is the closest voltage vector to $\boldsymbol{u}^*$ that satisfies the above requirements. However, this switch position cannot be used in the CMV-constrained problem, since it has $|u_o| = 2/3$. In that case, the switch position to be applied at $\theta = \frac{\pi}{6}$ will be the "000" one to satisfy the problem symmetries, see the appendix. However, when the modulation index is $m > \frac{2}{3}$, then the modulating signal is outside the inner hexagon. As a result, using the switch position "000" leads to a major deviation between the output and desired voltage, giving rise to significant current distortions.*

IV. Conclusions

This paper presented the computation of OPPs with constrained CMV. By appropriately imposing a constraint on the common-mode switch position, the CMV can be kept below a desired value, here at or below $\frac{V_{dc}}{6}$. Moreover, as demonstrated by the presented numerical results, by relaxing commonly made restrictions in the OPPs, such as quarter-wave symmetry, an increase in the current TDD is avoided and in some cases improved. Nevertheless, as observed and analyzed in this paper, this favorable behavior can be achieved only for even pulse numbers. Still, for odd pulse numbers the increase in the current TDD tends to be small when limiting the CMV.

Appendix

The CM switch position u_o, and thus the CMV v_o, inherit the symmetry properties of a three-phase OPP presented in Section II-A. Specifically, the following symmetry properties can be found in u_o.

Full-wave symmetry: Consider a three-phase OPP with property (P1). It follows that the CM switch position has a $\frac{2\pi}{3}$ periodicity, i.e., $u_o(\theta) = u_o\left(\theta + \frac{2\pi}{3}\right)\ \forall\theta \in \left[0, \frac{2\pi}{3}\right]$.

Proof.

$$\begin{aligned} u_o\left(\theta + \frac{2\pi}{3}\right) &= \frac{u(\theta + \frac{2\pi}{3}) + u(\theta) + u(\theta + \frac{4\pi}{3})}{3} \\ &= \frac{u(\theta + \frac{2\pi}{3}) + u(\theta) + u(\theta - \frac{2\pi}{3})}{3} \\ &= u_o(\theta) \end{aligned}$$

□

Half-wave symmetry: Consider a three-phase OPP with properties (P1) and (P2). As a result, the corresponding CM switch position has half-wave symmetry with period $\frac{2\pi}{3}$, i.e., $u_o(\theta) = -u_o\left(\theta + \frac{\pi}{3}\right)\ \forall\theta \in \left[0, \frac{\pi}{3}\right]$

Proof.

$$\begin{aligned} u_o\left(\theta + \frac{\pi}{3}\right) &= \frac{u(\theta + \frac{\pi}{3}) + u(\theta - \frac{\pi}{3}) + u(\theta + \pi)}{3} \\ &= \frac{u(\pi + \theta - \frac{2\pi}{3}) + u(\pi + \theta + \frac{2\pi}{3}) + u(\theta + \pi)}{3} \\ &= \frac{-u(\theta - \frac{2\pi}{3}) - u(\theta + \frac{2\pi}{3}) - u(\theta)}{3} \\ &= -u_o(\theta) \end{aligned}$$

□

Quarter-wave symmetry: Consider a three-phase OPP with properties (P1), (P2), and (P3). This implies that the CM switch position is a quarter-wave symmetric signal with period $\frac{2\pi}{3}$, i.e., $u_o(\theta) = u_o\left(\frac{\pi}{3} - \theta\right)\ \forall\theta \in \left[0, \frac{\pi}{6}\right]$

Proof.

$$\begin{aligned} u_o\left(\frac{\pi}{3} - \theta\right) &= \frac{u(\frac{\pi}{3} - \theta) + u(-\frac{\pi}{3} - \theta) + u(\pi - \theta)}{3} \\ &= \frac{u(\pi - \frac{2\pi}{3} - \theta) + u(\pi + \frac{2\pi}{3} - \theta) + u(\pi - \theta)}{3} \\ &= \frac{u(\theta + \frac{2\pi}{3}) + u(\theta - \frac{2\pi}{3}) + u(\theta)}{3} \\ &= u_o(\theta) \end{aligned}$$

□

It should be noted that these properties are also reflected in the sequence of voltage vectors in the $\alpha\beta$-plane. For demonstration purposes, consider the QaHWS OPP for $d = 4$ and $m = 0.8$. The single-phase QaHWS OPP u is shown in the top subfigure of Fig. 9, while the CM switch position u_o over

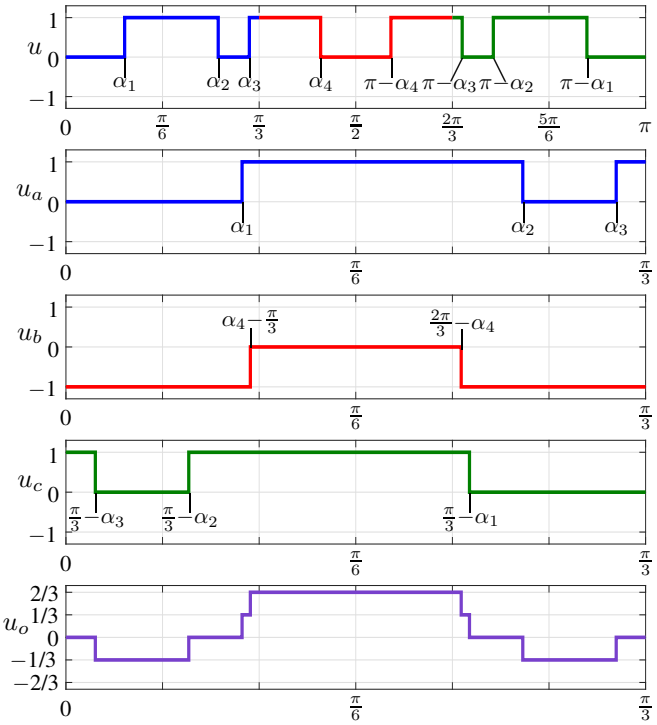

Fig. 9: Illustration of the calculation of the CM position u_o corresponding to the QaHWS OPP for $d = 4$ at modulation index $m = 0.8$

$\pi/3$ radians, i.e., a half of its fundamental period, is depicted in the bottom subfigure.[1] Finally, the three-phase OPP $\boldsymbol{u}_{abc}$ over a sixth of its fundamental period is shown in between the above-mentioned subfigures.

As can be seen, the sequence of switch positions of the three-phase OPP $\boldsymbol{u}_{abc}$ within the first $\pi/6$ radians is "$0-+$" $\xrightarrow{\text{at } \pi/3-\alpha_3}$ "$0-0$" $\xrightarrow{\text{at } \pi/3-\alpha_2}$ "$0-+$" $\xrightarrow{\text{at } \alpha_1}$ "$+-+$" $\xrightarrow{\text{at } \alpha_4-\pi/3}$ "$+0+$". The sequence of the corresponding voltage vectors is shown in Fig. 10 with blue colors. The sequence of switch positions of the three-phase OPP $\boldsymbol{u}_{abc}$ within the second $\pi/6$ radians is "$+0+$" $\xrightarrow{\text{at } 2\pi/3-\alpha_4}$ "$+-+$" $\xrightarrow{\text{at } \pi/3-\alpha_1}$ "$+-0$" $\xrightarrow{\text{at } \alpha_2}$ "$0-0$" $\xrightarrow{\text{at } \alpha_3}$ "$+-0$", see also Fig. 10 where the sequence of corresponding voltage vectors is shown with green colors. We observe that these two sequences are symmetric as they are mirrored with respect to the axis aligned with the short vectors that correspond to the switch positions "$0-0$" and "$+0+$" as well as the long vector resulting from the switch position "$+-+$". This means that the sequence of voltage vectors in the first quarter of the fundamental period of the CM switch position must end in one of the voltage vectors on the said symmetry axis.

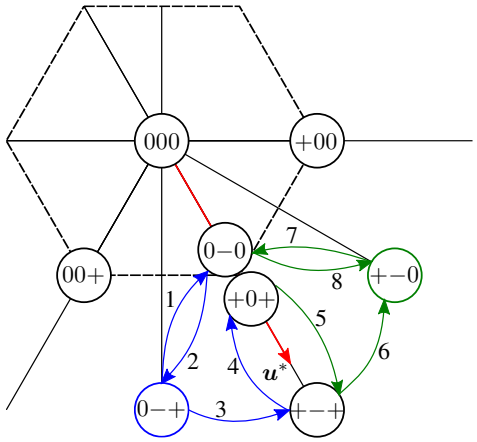

Fig. 10: Sequence of voltage vectors of the three-phase OPP in Fig. 9 over a sixth of the fundamental period. Note that $\boldsymbol{u}^*$ denotes the fundamental component of the OPP in the $\alpha\beta$-plane.

References

[1] A. Mütze and A. Binder, "Don't lose your bearings—Mitigation techniques for bearing currents in inverter-supplied drive systems," *IEEE Ind. Appl. Mag.*, vol. 12, no. 4, pp. 22–31, Jul./Aug. 2006.

[2] L. Kai, J. Zhao, W. Wu, M. Li, L. Ma, and G. Zhang, "Performance analysis of zero common-mode voltage pulse-width modulation techniques for three-level neutral point clamped inverters," *IET Power Electron.*, vol. 9, no. 14, pp. 2654–2664, Nov. 2016.

[3] H.-J. Kim, H.-D. Lee, and S.-K. Sul, "A new PWM strategy for common-mode voltage reduction in neutral-point-clamped inverter-fed ac motor drives," *IEEE Trans. Ind. Appl.*, vol. 37, no. 6, pp. 1840–1845, Nov./Dec. 2001.

[4] M. M. Renge and H. M. Suryawanshi, "Multilevel inverter to reduce common mode voltage in ac motor drives using SPWM technique," *J. Power Electron.*, vol. 11, no. 1, pp. 21–27, Jan. 2011.

[5] M.-J. Tsai, H.-C. Chen, M.-R. Tsai, Y.-B. Wang, and P.-T. Cheng, "Evaluation of carrier-based modulation techniques with common-mode voltage reduction for neutral point clamped converter," *IEEE Trans. Power Electron.*, vol. 33, no. 4, pp. 3268–3275, Apr. 2018.

[6] A. M. Hava and E. Ün, "Performance analysis of reduced common-mode voltage PWM methods and comparison with standard PWM methods for three-phase voltage-source inverters," *IEEE Trans. Power Electron.*, vol. 24, no. 1, pp. 241–252, Jan. 2009.

[7] K. D. Pham and N. V. Nguyen, "A reduced common-mode-voltage pulsewidth modulation method with output harmonic distortion minimization for three-level neutral-point-clamped inverters," *IEEE Trans. Power Electron.*, vol. 35, no. 7, pp. 6944–6962, Jul. 2020.

[8] Z. Zhao, Y. Zhong, H. Gao, L. Yuan, and T. Lu, "Hybrid selective harmonic elimination PWM for common-mode voltage reduction in three-level neutral-point-clamped inverters for variable speed induction drives," *IEEE Trans. Power Electron.*, vol. 27, no. 3, pp. 1152–1158, Mar. 2012.

[9] G. S. Buja and G. B. Indri, "Optimal pulsewidth modulation for feeding ac motors," *IEEE Trans. Ind. Appl.*, vol. IA-13, no. 1, pp. 38–44, Jan. 1977.

[10] I. Tsoumas, "On the computation of optimized pulse patterns with zero common mode voltage," in *Proc. Eur. Conf. on Power Electron. and Applicat.*, Genova, Italy, Sep. 2019, pp. P.1–P.10.

[11] P. Hokayem, I. Pejcic, and N. Oikonomou, "Optimal current trajectories for power converters with minimal common mode voltage," *IFAC World Congr.*, vol. 50, no. 1, pp. 2107–2112, Jul. 2017.

[12] A. Birth, T. Geyer, H. d. T. Mouton, and M. Dorfling, "Generalized three-level optimal pulse patterns with lower harmonic distortion," *IEEE Trans. Power Electron.*, vol. 35, no. 6, pp. 5741–5752, Jun. 2020.

[1] Note that due to the QaHWS of the OPP, the full information of u_o is included in $\pi/6$ radians. For illustration purposes, however, the CM switch position is depicted for half of its fundamental period.